

# Dysfunction of Endocytic and Autophagic Pathways in a Lysosomal Storage Disease

Tokiko Fukuda, MD, PhD,<sup>1</sup> Lindsay Ewan, BA,<sup>1</sup> Martina Bauer, BA,<sup>1</sup> Robert J. Mattaliano, PhD,<sup>2</sup> Kristien Zaal, PhD,<sup>3</sup> Evelyn Ralston, PhD,<sup>3</sup> Paul H. Plotz, MD,<sup>1</sup> and Nina Raben, MD, PhD<sup>1</sup>

**Objective:** To understand the mechanisms of skeletal muscle destruction and resistance to enzyme replacement therapy in Pompe disease, a deficiency of lysosomal acid  $\alpha$ -glucosidase (GAA), in which glycogen accumulates in lysosomes primarily in cardiac and skeletal muscles. **Methods:** We have analyzed compartments of the lysosomal degradative pathway in GAA-deficient myoblasts and single type I and type II muscle fibers isolated from wild-type, untreated, and enzyme replacement therapy-treated GAA knock-out mice. **Results:** Studies in myoblasts from GAA knock-out mice showed a dramatic expansion of vesicles of the endocytic/autophagic pathways, decreased vesicular movement in overcrowded cells, and an acidification defect in a subset of late endosomes/lysosomes. Analysis by confocal microscopy of isolated muscle fibers demonstrated that the consequences of the lysosomal glycogen accumulation are strikingly different in type I and II muscle fibers. Only type II fibers, which are the most resistant to therapy, contain large regions of autophagic buildup that span the entire length of the fibers. **Interpretation:** The vastly increased autophagic buildup may be responsible for skeletal muscle damage and prevent efficient trafficking of replacement enzyme to lysosomes.

Ann Neurol 2006;59:700–708

The pathological hallmark of Pompe disease (glycogen storage disease type II), an autosomal recessive disorder caused by the deficiency of lysosomal acid  $\alpha$ -glucosidase (GAA), is the accumulation of glycogen primarily in cardiac and skeletal muscles.<sup>1</sup> Complete GAA deficiency causes a rapidly progressive disease in infants who invariably die of cardiac failure within the first 2 years of life.<sup>2</sup> In less severe late-onset forms, cardiac muscle is usually spared; slowly progressive myopathy and diaphragmatic weakness are the main symptoms.<sup>3</sup>

Enzyme replacement therapy (ERT) with recombinant human enzyme (rhGAA) is being investigated in clinical trials. In ERT, the rhGAA propeptide is endocytosed and delivered to the acidic milieu of lysosomes. Uptake of the rhGAA at the plasma membrane is mediated by the cation-independent mannose-6-phosphate receptor (CI-MPR).<sup>4</sup> The protein bound to the receptor is concentrated in clathrin-coated pits; it subsequently enters a chain of endocytic vesicles, which participate in recycling and sorting the enzyme. The acidic pH of the late endosomes causes the release of the enzyme, after which the receptor is recycled for ad-

ditional rounds of sorting, whereas the enzyme moves on to the lysosomes for the final maturation.<sup>5,6</sup>

For Pompe's disease, the effective clearance of skeletal muscle glycogen, as indicated by both animal preclinical<sup>7–10</sup> and human clinical studies,<sup>11–14</sup> appears to be significantly more difficult than anticipated. Neither transgenic liver-secreted hGAA nor even transgenic hGAA expressed in the skeletal muscle of knock-out (KO) mice have been successful.<sup>8,10</sup> In the mouse model, type II skeletal muscle was most resistant to therapy.<sup>9,10</sup> This outcome of ERT has highlighted the gaps in knowledge of the pathogenesis of the disease. Although the primary defect in Pompe disease has been long established, intralysosomal glycogen storage, little is known about the secondary events responsible for muscle weakness and wasting. In fact, little is known about the lysosomal system in skeletal muscle, healthy or diseased.

We report here analyses of the downstream pathways that are affected as a result of the accumulation of undigested substrate in lysosomes. Studies in KO myoblasts have shown that the deficiency of a single lysosomal enzyme results in a global vacuolar dysfunction

From the <sup>1</sup>Arthritis and Rheumatism Branch, National Institute of Arthritis and Musculoskeletal and Skin Diseases, National Institutes of Health, Bethesda, MD; <sup>2</sup>Cell and Protein Therapeutics R&D, Genzyme Corporation, Framingham, MA; and <sup>3</sup>Light Imaging Section, Office of Science and Technology, National Institute of Arthritis and Musculoskeletal and Skin Diseases, National Institutes of Health, Bethesda, MD.

Received Sep 12, 2005, and in revised form Dec 15. Accepted for publication Dec 26, 2005.

Published online Mar 10, 2006 in Wiley InterScience (www.interscience.wiley.com). DOI: 10.1002/ana.20807

Address correspondence Dr Raben, 9000 Rockville Pike, Clinical Center Building 10/9N244, NIH, NIAMS, Bethesda, MD 20892-1820. E-mail: rabenn@arb.niams.nih.gov

and abnormal vesicular trafficking of both the endocytic and autophagic pathways. Experiments using single muscle fibers isolated from type I- and type II-rich muscles from KO mice emphasize the role of the autophagic pathway in the pathogenesis of the disease and shed new light on both muscle wasting and the resistance to ERT.

## Materials and Methods

### Antibodies

The following primary and secondary antibodies were used: anti-Lamp1 (lysosome-associated membrane protein 1; BD Pharmingen, San Diego, CA); anti-EEA1 (early endosomes antigen 1; Affinity BioReagents, Golden, CO); anti-CI-MPR (a gift from Dr W. Gregory, University of Washington, Seattle, WA); anti-TfR (transferrin receptor; Zymed Laboratories, San Francisco, CA); anti-GGA2 (Golgi-localized  $\gamma$ -ear-containing, Arf-binding protein 2), anti-GAPDH (glyceraldehyde phosphate dehydrogenase; Abcam, Cambridge, MA); anti-AP-1 (adaptor protein 1), anti-GM130 (BD Transduction Laboratories, San Jose, CA); anti-LC3 (microtubule-associated protein 1 light chain 3; a gift from Dr T. Ueno, Juntendo University School of Medicine, Japan); anti- $\alpha$  tubulin, anti-vinculin (Sigma-Aldrich, St. Louis, MO); Alexa Fluor-conjugated secondary antibodies (Invitrogen, La Jolla, CA); and nanogold-conjugated secondary antibodies (Nanoprobes, Yaphank, NY).

### Primary Mouse Myoblast Cultures and Gene Transfection

Primary mouse myoblasts were prepared and enriched by several rounds of preplating as described.<sup>15</sup> Myoblasts were transiently transfected with pEGFP-LC3, pEGFP-Rab5, or pEGFP-Lamp1 using the FuGENE 6 reagents according to the manufacturer's instructions. The cells were analyzed 48 to 72 hours after transfection by confocal microscopy (Zeiss LSM 510 META; Zeiss, Oberkochen, Germany).

### Single Muscle Fiber Preparation

Fibers were prepared from wild-type (WT), untreated, or ERT-treated KO mice.<sup>16</sup> The mice were 4 months old at start of therapy. They received the rhGAA (20mg/kg twice a week; Genzyme, Cambridge, MA) for up to 6 months. Soleus (predominantly type I) and white gastrocnemius (predominantly type IIB) muscles were fixed with 2% paraformaldehyde for 1 hour, followed by fixation in methanol ( $-20^{\circ}\text{C}$ ) for 6 minutes. After several rinses, single fibers were obtained by manual teasing.

### Immunofluorescence Microscopy and Western Analysis

Paraformaldehyde-fixed myoblasts or single muscle fibers were immunostained with markers for endocytic/autophagic compartments according to the standard procedures. The cells and fibers were analyzed by confocal microscopy. Western analyses of the tissue lysates were performed as described elsewhere.<sup>10</sup>

### pH Measurements

The late endosome/lysosome pH assay is based on measuring the ratio of pH-sensitive fluorescein (FL) to pH-insensitive TMR (tetramethylrhodamine) fluorescence emissions. Myoblasts were incubated with FL/TMR double-conjugated dextran overnight, followed by 2- or 36-hour chase. Cross talk-free confocal images of cells were recorded using the appropriate emission ranges. The FL/TMR ratio of individual dextran containing vesicles was calculated. This ratio, dependent on pH, but not dye concentration,<sup>17</sup> was converted to a pH value as described.<sup>18</sup>

### Electron Microscopy

For electron microscopy (EM), muscles were fixed in 2% glutaraldehyde/2% paraformaldehyde/0.1M sodium cacodylate. For immunogold EM, single fibers were fixed with paraformaldehyde only and stained for Lamp1, and nanogold-conjugated secondary antibodies were used as described elsewhere.<sup>19</sup> Small pieces of muscle or single fibers were observed in a Jeol 1200 microscope (JEOL, Peabody, MA) at 60kV.

### Image Analysis

The mobility of late endocytic vesicles was analyzed by Colocalization Orthogonal Regression algorithm (<http://mipav.cit.nih.gov>). Data are given as mean  $\pm$  standard deviation or as median and interquartile. Student's *t* test was used for statistical analysis. Whiskers within a box plot indicate range within 1.5-interquartile range; open circles represent data points between 1.5- and 3-interquartile range, and plus signs represent extreme data points.

Animal care and experiments were conducted in accordance with the National Institutes of Health Guide for the Care and Use of Laboratory Animals.

## Results

### Expansion of Endocytic and Autophagic Vesicles, Abnormalities in Lysosomal pH, and Decreased Vesicle Mobility in Knock-out Myoblasts

Transfection with or immunostaining for lysosomal (Lamp1), late endosomal (Lamp1/CI-MPR; CI-MPR is present on late endosomes, but not on lysosomes<sup>20</sup>) markers, or early endosomal (Rab5 and EEA1) markers showed a significant expansion of the endocytic vesicles in KO myoblasts (Figs 1A–F). The autophagic vacuoles identified by transfection with GFP-LC3 (an autophagosomal marker<sup>21</sup>) were also strikingly increased in size in the diseased cells (see Fig 1G).

To examine the acidification of the expanded late endocytic vesicles in the KO, we exposed the cells to FL/TMR double-conjugated dextran for 24 hours followed by 2-hour chase. In the WT myoblasts, most of the dextran accumulated in the vesicles with normal lysosomal pH<sup>22</sup> of less than 5.2 (median value, 4.74). In contrast, in KO only approximately 60% of vesicles were within the normal lysosomal pH range (median value, 5.08; Table). Furthermore, the difference persisted after 36-hour chase, suggesting that a subset of

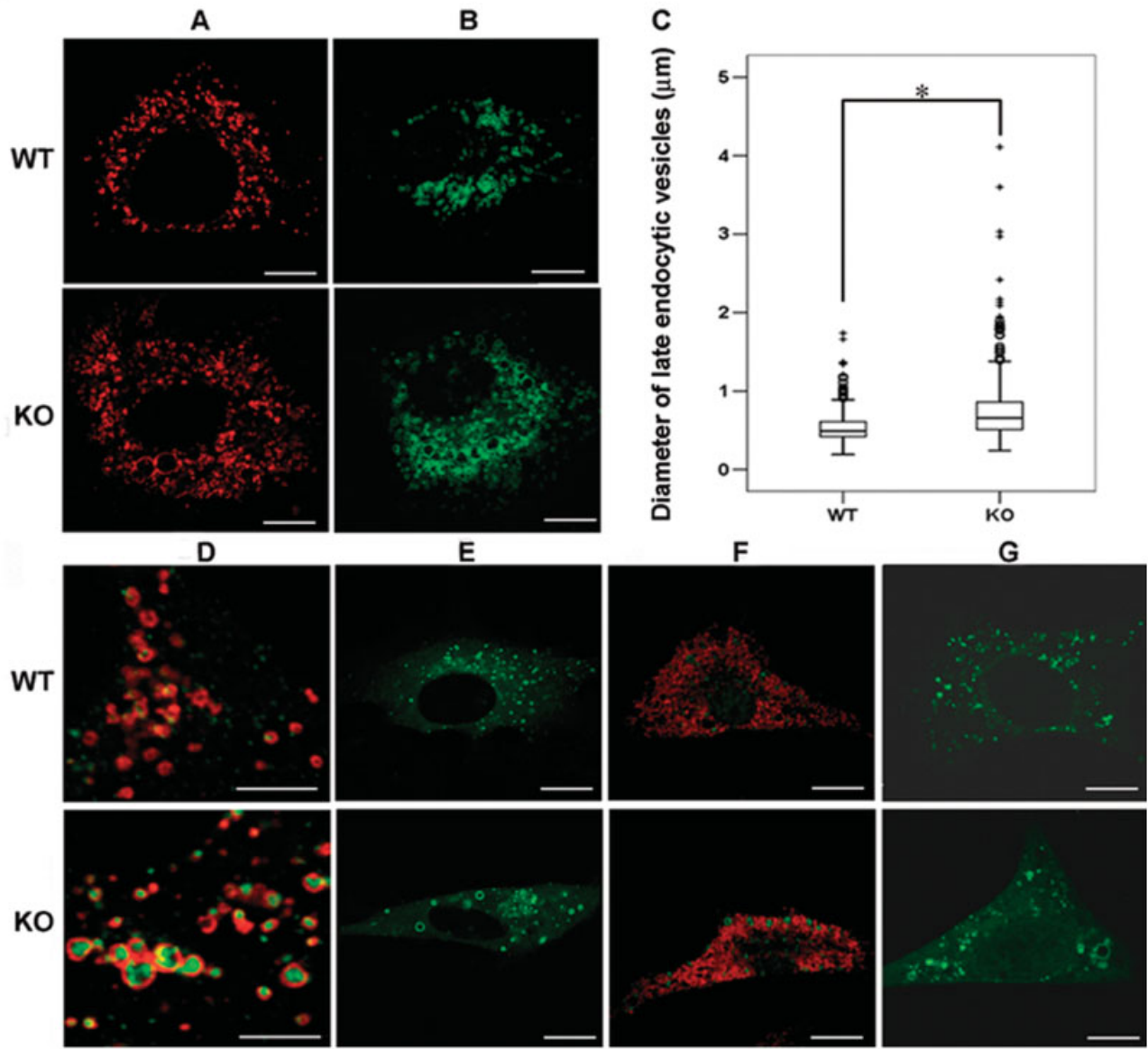


Fig 1. Confocal images of myoblasts stained for Lamp1 (lysosome-associated membrane protein 1) (A) or transfected with GFP-Lamp1 (B) showing the enlargement of late endosomes/lysosomes in knock-out (KO) animals. (C) The diameter of vesicles in wild-type (WT) and KO cells is different: median values are 0.49 and 0.66 μm respectively; \* $p < 0.05$  (>1,000 vesicles were analyzed). (D) The enlargement of late endosomes in KO is confirmed by the size of Lamp1 (red)/cation-independent mannose-6-phosphate receptor (CI-MPR) (green) double-positive structures. (E, F) The enlargement of early endosomes in KO cells is shown by transfection with GFP-Rab5 (E) or by staining for early endosomes antigen 1 (EEA1) (green)/Lamp1 (red). (G) The enlargement of autophagic vacuoles (AVs) in KO cells is shown by transfection with GFP-LC3. Bars = 10 μm (A, B, E-G); 5 μm (D).

alkalinized lysosomes is present in KO myoblasts. Nevertheless, the number of vesicles within the normal lysosomal pH range increased after 36-hour chase, indicating that the transport from late endosomes to lysosomes may pose an additional problem in the KO animals (see the Table). Indeed, decreased mobility of the enlarged late endocytic compartments in KO cells was shown by imaging of living GFP-Lamp1-transfected myoblasts. The mobile late endosomes/lysosomes occupied approximately 30% of the total late

endosomal/lysosomal area in the WT cells, whereas the percentage was only approximately 18% in the KO cells (Fig 2).

#### Differential Effect of Enzyme Replacement Therapy in Types I and II Muscle Fibers in Knock-out Mice

Next, we analyzed vesicles of the endocytic pathway in isolated muscle fibers of WT and KO mice and the effect of ERT. Our initial studies indicated that ERT cleared glycogen from type I-rich muscle more effi-

Table. Percentage of Fluorescein/Tetramethylrhodamine Dextran-Labeled Vesicles Classified by pH

| Cell Type/Chase Period <sup>a</sup> | pH range |                |          |
|-------------------------------------|----------|----------------|----------|
|                                     | pH < 5.2 | 5.2 ≤ pH ≤ 5.8 | pH > 5.8 |
| WT/2 hours                          | 89.0     | 9.1            | 1.9      |
| KO/2 hours                          | 60.3     | 26.5           | 13.2     |
| WT/36 hours                         | 90.4     | 5.0            | 4.6      |
| KO/36 hours                         | 70.2     | 18.5           | 11.3     |

<sup>a</sup>The number of vesicles analyzed: approximately 1,400 (WT/2 hours); approximately 1,300 (KO/2 hours); approximately 600 (WT/36 hours and KO/36 hours each).

KO = knock-out; WT = wild type.

ciently than from type II-rich muscle, despite the higher level of glycogen accumulation in untreated type I-rich muscles.<sup>9,10</sup> Confocal images of Lamp1-immunostained single fibers confirmed that type II fibers responded poorly to ERT (Fig 3). We have tried, therefore, to identify the characteristics of the two fiber types that may account for the different responses to therapy.

#### Expansion of Endocytic Vesicles and Fiber-Type Specific Distribution of Lysosomes

As in KO myoblasts, enlarged endosomes/lysosomes were found in both fiber types of untreated KO mice (not shown). Confocal images, however, showed major differences in the distribution of lysosomes in types I and II WT fibers (see Figs 3 and 4). The lysosomes in type I fibers are arranged in long stretches, whereas in type IIB fibers they are not. The expansion of long stretches of lysosomes in type I KO fibers generates a tube-like structure (see Figs 4A, C; n = 70). In contrast, in type IIB KO fibers, the expanded lysosomes are distributed throughout the fibers and are not connected (see Fig 4B; n = 200). Lamp1/GM130 (*cis*-Golgi complex marker) double staining showed the two organelles positioned next to one another in types I and II WT fibers, as well as in type I KO fibers. In contrast, the distribution of Golgi marker in type II KO fibers was less regular and the association with the lysosomes was not entirely maintained (see Fig 4B).

#### Autophagic Buildup and Atrophy in Type II Fibers of Knock-out Mice

Confocal microscopy of single type I KO fibers showed isolated LC3-positive structures (not shown), and EM captured occasional double-membrane autophagosomes (Fig 5A). Autophagic buildup, however, occurred only in type II KO fibers. The autophagic regions contained vesicles with morphological features representative of various stages of the autophagic process (see Fig 5B).

None of the Lamp1-positive structures initially observed in immunofluorescence (see Fig 3) remotely approached the size of these autophagic areas. Closer ex-

amination of type II fibers showed long areas of LC3/Lamp1 double-positive structures connected by a dark area devoid of fluorescence (Figs 6B, C) or connected by diffuse Lamp1 staining (see Figs 6D, E, H). The myofibrillar striations appeared to be disrupted in these regions (see Figs 6B, C). As shown by immunogold EM (see Figs 5C, D), all large vesicles in type I fibers are lined with dark grains (see Fig 5C, arrows); in contrast, the autophagic buildup areas in type II fibers contain discrete Lamp1-positive smaller vesicles (see Fig 5D, arrowhead).

Once discovered, the areas of autophagic buildup were found easily. They extend for nearly the length of the fibers (see Fig 6H) and are sometimes branched (see Fig 6D). Importantly, they were not removed by ERT (not shown). Staining with  $\alpha$ -tubulin showed disorganization of the microtubular structure in the autophagic areas (Fig 7).

In addition, there was a dramatic reduction in the size of type II KO fibers compared with the WT (see Figs 3 and 6). The average diameter of a type II fiber of 8- to 10-month-old WT mice was  $90.9 \pm 16.5 \mu\text{m}$  (n = 70) compared with  $56.9 \pm 11.9 \mu\text{m}$  (n = 59;  $p < 0.0001$ ) and  $54.3 \pm 14.3 \mu\text{m}$  (n = 41) for fibers from age-matched untreated and ERT-treated mice, respectively. In contrast, type I fibers showed a tendency for hypertrophy: the average fiber size in 8- to 10-month-old KO mice was  $64.2 \pm 12.3 \mu\text{m}$  (n = 25) compared with  $57.7 \pm 10.5 \mu\text{m}$  (n = 33) in age-matched WT mice.

#### Low Abundance of Trafficking Proteins in Type II-Rich Muscle

Levels of trafficking proteins also differ between fiber types in both the WT and KO mice. In addition to the reduced levels of CI-MPR, clathrin, and AP-2 shown previously,<sup>10</sup> the TfR, GGA2, and AP-1 (Fig 8) are all less abundant in type II than in type I muscle. In fact, GGA2 was virtually absent in type II muscle, and AP-1, a negative regulator of CI-MPR-mediated endocytosis, was upregulated in type II but not type I KO muscle (see Fig 8).

#### Discussion

We have found an expansion of all the vesicles of the endosomal/lysosomal system (rather than just the lysosomes) and a striking decrease in the mobility of these vesicles in KO myoblasts, suggesting that vesicular fusion may be impaired. Because efficient targeting and processing of lysosomal enzymes requires a proper pH gradient along the endocytic pathway,<sup>22,23</sup> we considered that the enlargement and stasis of all the endocytic compartments might alter pH, thereby preventing the dissociation of rhGAA from the receptor and/or inhibiting the enzyme activity. The dissociation of the MPR-ligand complexes on late endosomes requires a

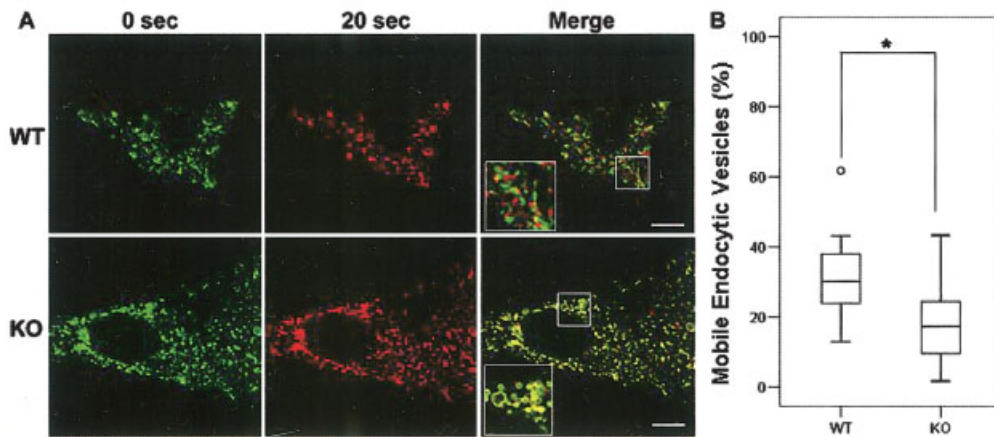


Fig 2. Reduced mobility of late endocytic vesicles in knock-out (KO) myoblasts. (A) Images of live GFP-lysosome-associated membrane protein 1 (Lamp1)-transfected cells at time 0 (pseudo-green) and 20 seconds (pseudo-red). In the merged images, particles that have moved are red. The amount of red is significantly higher in WT than in KO. Bars = 10 $\mu$ m. (B) Quantitative analysis of vesicle mobility (10 WT and 10 KO cells were used) was done by calculating the percentage of red area in the merged images relative to the total late endosomal/lysosomal area.

pH below 6.0.<sup>24</sup> The inability of the CI-MPR to dissociate from procathepsin D resulting from a profound acidification defect has been found in certain cancer cells.<sup>25</sup> Elevated intralysosomal pH has been described in other lysosomal storage diseases, such as mucopolisodosis type IV and several forms of neuronal lipofuscinoses.<sup>26,27</sup> Despite a significant expansion of the endocytic vesicles, the majority of late endosomes/lysosomes maintained normal pH in Pompe cells. There was, however, an increased population of vesicles with pH above the normal lysosomal and even late endosomal

range, suggesting a defective acidification of a subset of the late endosomes/lysosomes that may be of pathogenic importance in multinucleated muscle fibers.

We have identified some intrinsic properties of types I and II fibers that might contribute to their differential response to ERT. The levels of proteins involved in receptor-mediated endocytosis and trafficking of lysosomal enzymes are much lower in type II than in type I fibers in both WT and KO animals. These proteins include (but are not limited to) the CI-MPR, clathrin, AP-2 complex, TfR (a marker for recycling endosomes),

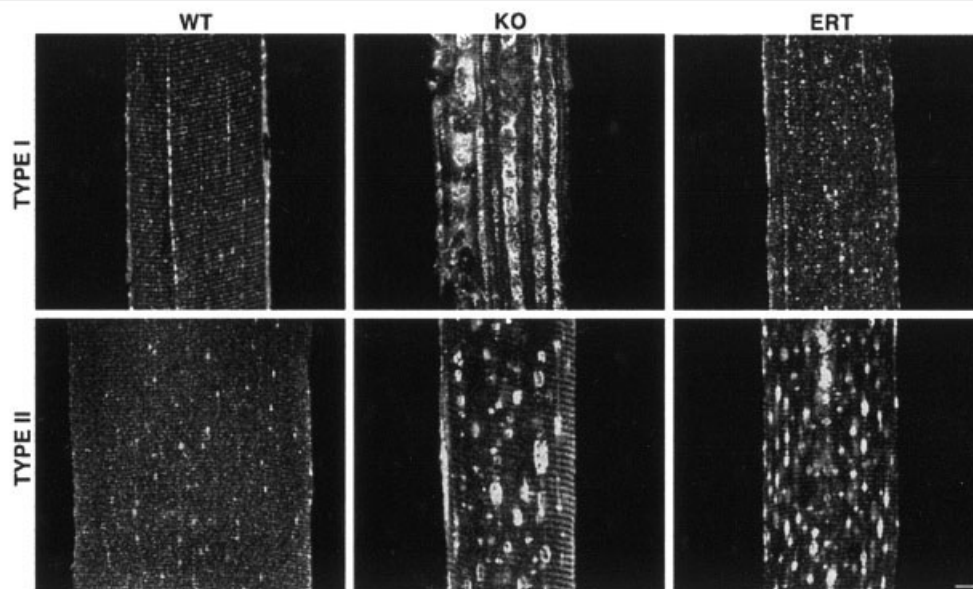


Fig 3. Confocal images of type I (6-month-old mice) and type IIB (10-month-old mice) fibers stained for lysosome-associated membrane protein 1 (Lamp1). After 2 months of therapy the size of lysosomes in type I knock-out (KO) fibers is similar to that in wild-type (WT) fibers. The lysosomes remain significantly enlarged in type II KO fibers after 6 months of therapy. Bar = 10 $\mu$ m.

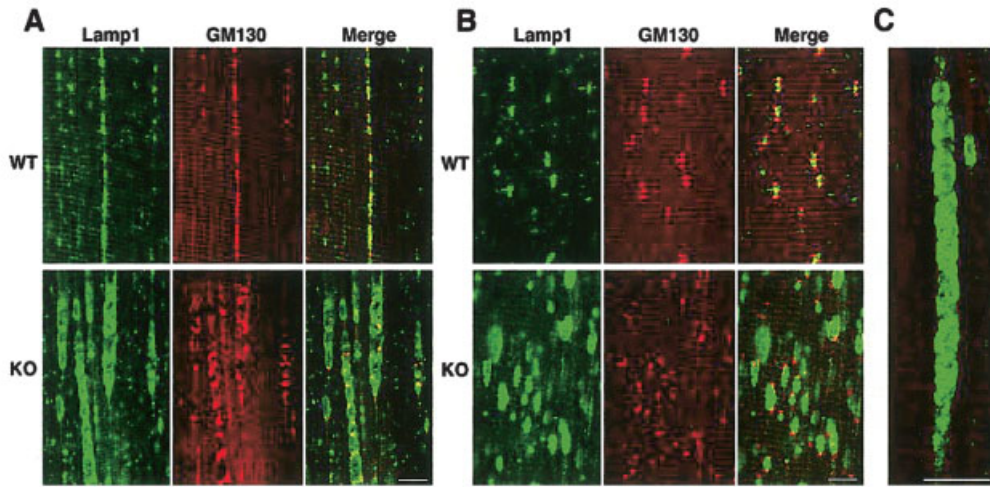


Fig 4. Confocal microscopy of lysosome-associated membrane protein 1 (Lamp1)/GM130 double-stained fibers showing closely apposed or fused enlarged lysosomes in type I knock-out (KO) fibers (A) and lysosomes that remain apart in type II KO fibers (B). The distribution of the Golgi complex elements (GM130 in A and B) is different in type I and type II fibers in wild-type fibers (WT). A similar fiber-type-specific distribution of the Golgi marker was described in normal rat muscle.<sup>45,46</sup> This marker remained aligned in type I KO fibers as in WT, whereas in type II KO fibers, the Golgi marker appeared irregular. (C) Interconnected tube-like structure in type I KO fiber (Lamp1 staining). Bars = 10 $\mu$ m.

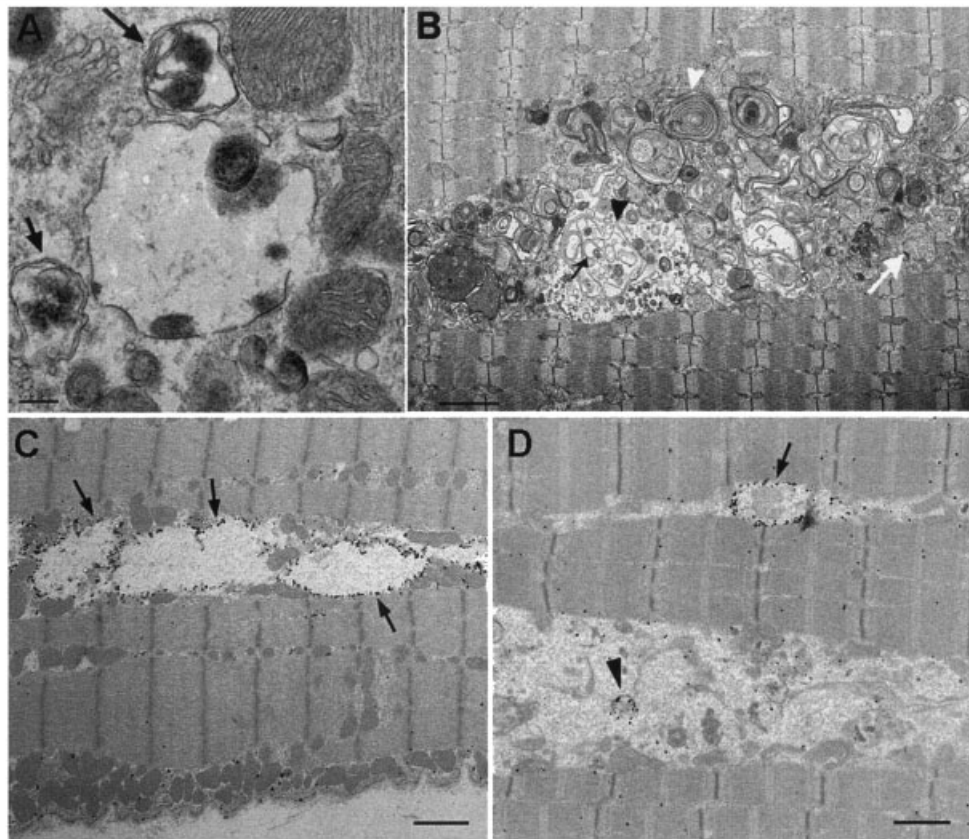


Fig 5. Electron microscopy (EM) of types I and II fibers from 10-month-old knock-out (KO) mice. (A) Double-membrane autophagosomes in type I fiber. (B) Autophagic buildup in type II fiber: autophagosome (black arrow); large autophagic vacuole (AVs) containing small autophagosomes (black arrowhead); multivesicular body (white arrow); multimembrane structure (white arrowhead). Types I (C) and II fibers (D) labeled with lysosome-associated membrane protein 1 (Lamp1) for immunogold EM showing strong labeling on lysosomal membranes (arrows) and discrete smaller Lamp1-positive vesicle within the area of autophagic buildup in type II fiber (arrowhead). Bars = 0.2 $\mu$ m (A); 2 $\mu$ m (B); 1 $\mu$ m (C, D).

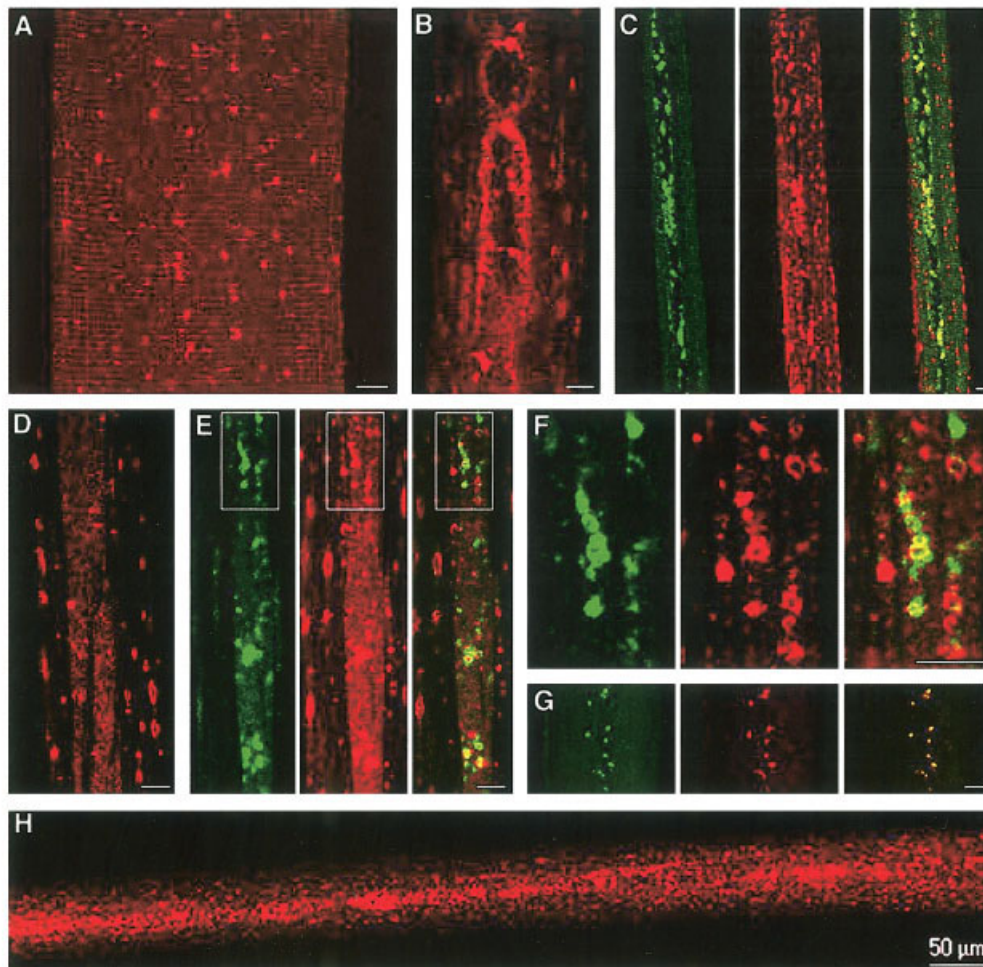


Fig 6. Autophagic buildup in type II fibers from knock-out (KO) mice. Confocal microscopy of type II fibers from wild-type (WT) (A) and KO (B–F, H) mice stained for lysosome-associated membrane protein 1 (Lamp1) alone (red) or together with LC3 (green) (C, E, F), showing large central region of autophagy in each fiber. The areas of autophagic buildup appear either as a huge “black hole” (B, C) or as a diffuse Lamp1 staining (D, E). (F) Enlarged view of autophagosomes (green) colocalized with late endosomes/lysosomes (red). (G) Unstained KO fibers show autofluorescence in the autophagic area. (H) Lamp1 immunostaining of type II KO fiber showing that the autophagic buildup spans the length of the core of a fiber. Bars = 10  $\mu\text{m}$  (A–G).

and a family of GGA proteins, which link cargo molecules and clathrin-coated vesicle assembly at the *trans*-Golgi network and early endosomes.<sup>28–30</sup> Interestingly, the level of another protein involved in vesicle transport, Vear, was shown to be much lower in type II than in type I fibers in humans.<sup>31</sup> However, one of the trafficking proteins, AP-1, was upregulated in type II KO fibers compared with WT. Paradoxically, this upregulation may negatively affect the CI-MPR-mediated endocytosis.<sup>32</sup> In addition to the low level of trafficking proteins, the distribution and organization of the lysosomes may also be disadvantageous for type II fibers.

The overcrowding and stasis observed in KO is exacerbated by an increase in size of autophagic vacuoles in both fiber types. Autophagy is a highly regulated process in which parts of the cytoplasm and organelles are sequestered within double-membrane-limited auto-

phagosomes.<sup>33,34</sup> The autophagosomes mature and become amphisomes and autolysosomes when they fuse with endosomes or lysosomes.<sup>35,36</sup> Excessive autophagy is a hallmark of several myopathies including Pompe disease; accumulation of autophagic vacuoles has been documented both in patients and in the KO models.<sup>10,37,38</sup> It has been suggested that the autophagic clusters (referred to as “noncontractile” material), observed in some myofibrils by EM, may contribute to the age-related decline in muscle contractile function in Pompe disease mice.<sup>38,39</sup>

Nutritional deprivation induces autophagy, presumably to provide substrates for energy. An increase in autophagy in Pompe skeletal muscle raises an intriguing possibility that the failure to digest lysosomal glycogen to glucose, the fundamental lesion in Pompe disease, may set up a vicious cycle by depriving muscle

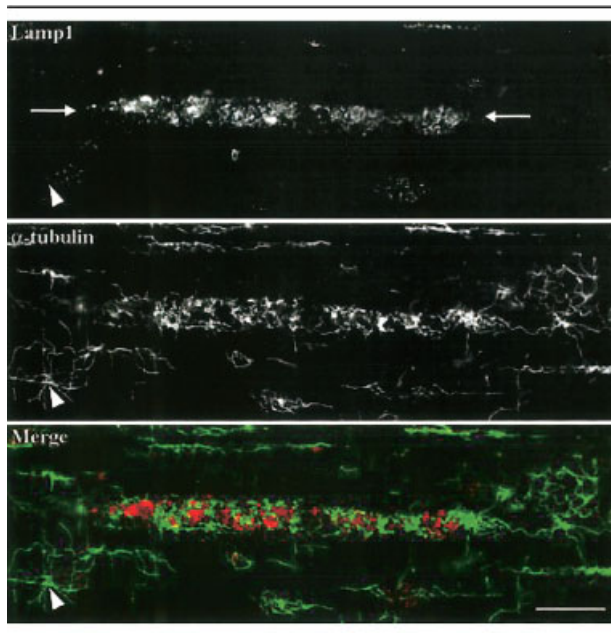


Fig 7. Confocal microscopy of type II fiber double-stained for lysosome-associated membrane protein 1 (Lamp1) and  $\alpha$ -tubulin showing disorganization of microtubule network in the area of autophagic buildup (flanked by arrows in Lamp1 image) compared with that in the neighboring area (arrowheads). Bar = 10 $\mu$ m.

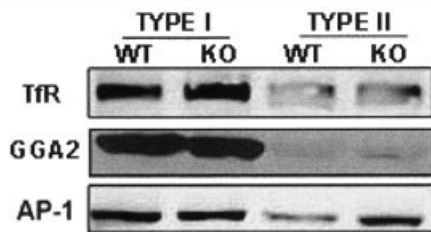


Fig 8. Western analysis of proteins involved in clathrin-mediated endocytosis in types I and II muscle fibers. Glyceraldehyde phosphate dehydrogenase (GAPDH) was used as loading control for transferrin receptor (TfR) and adaptor protein 1 (AP-1), and vinculin was used for Golgi-localized  $\gamma$ -ear-containing, Arf-binding protein (GGA2) (not shown).

cells of a necessary source of energy. Glucose deprivation in rat cardiomyocyte, for example, results in autophagic rather than apoptotic cell death.<sup>40</sup> Only in type II KO fibers, however, did we see huge autophagic masses (the full extent of which is best seen by confocal microscopy) both before and after ERT, suggesting that the pathogenesis of the disease in the two fiber types is quite different. The role of GAA in type II fibers may resemble that in liver and heart in the immediate postnatal period when there is a demand for massive liberation of glucose. During this period, GAA activity increases dramatically, and the autophagosomal-lysosomal degradation of glycogen to glucose provides energy to meet the metabolic requirements.<sup>41</sup>

The enormous autophagic buildup in glycolytic type II, but not oxidative type I, fibers from the KO mice may reflect both a more robust increase in autophagy and an impairment of fusion of autophagic vacuoles with endosomes/lysosomes. Indeed, significantly increased autophagy in response to starvation was observed in type II, but not in type I, muscle in transgenic mice overexpressing GFP-LC3.<sup>42</sup>

We suggest, therefore, that the pathological cascade, triggered in response to the primary defect in type II glycolytic fibers, may be as follows: the failure of glycogen digestion results in a local starvation that stimulates a strong autophagic response that, coupled with the inability of the vesicles to fuse and discharge their contents in the lysosomes, leads to a continuous autophagic buildup and a profound disorganization of the microtubule structure that may perpetuate the autophagic process.<sup>43</sup>

There is a clear need to improve the treatment of Pompe affected skeletal muscle. Although remodeling the carbohydrate of rhGAA to increase its affinity for CI-MPR was shown to enhance the efficacy of the ERT in KO mice,<sup>44</sup> the secondary changes in vesicle trafficking and autophagy are likely to compromise the ability of the fibers to recover. Consequently, therapeutic efforts to switch fiber type or to find an alternative route to provide energy to type II fibers should be sought.

This research was supported by the Intramural Research Program of the NIH (National Institute of Arthritis and Musculoskeletal and Skin Diseases [NIAMS]).

We thank Drs K. Wang and R. L. Proia for helpful discussions, Dr K. Nagashima, J-H. Tao-Cheng, and V. Tanner-Crocker for help with the electron microscopy. We also thank Drs T. Yoshimori, P. Stahl, and G. Patterson for providing some of the plasmids for transfection experiments.

## References

- Hirschhorn R, Reuser AJ. Glycogen storage disease type II: acid alpha-glucosidase (acid maltase) deficiency. In: The metabolic and molecular basis of inherited disease. Scriver CR, Beaudet AL, Sly WS, Valle D, eds. New York: McGraw-Hill, 2001: 3389–3420.
- van den Hout HM, Hop W, van Diggelen OP, et al. The natural course of infantile Pompe's disease: 20 original cases compared with 133 cases from the literature. *Pediatrics* 2003;112: 332–340.
- Hagemans ML, Winkel LP, Van Doorn PA, et al. Clinical manifestation and natural course of late-onset Pompe's disease in 54 Dutch patients. *Brain* 2005;128:671–677.
- Van der Ploeg AT, Kroos MA, Willemsen R, et al. Intravenous administration of phosphorylated acid alpha-glucosidase leads to uptake of enzyme in heart and skeletal muscle of mice. *J Clin Invest* 1991;87:513–518.
- Wisselaar HA, Kroos MA, Hermans MM, et al. Structural and functional changes of lysosomal acid alpha-glucosidase during intracellular transport and maturation. *J Biol Chem* 1993;268: 2223–2231.

6. Moreland RJ, Jin X, Zhang XK, et al. Lysosomal acid alpha-glucosidase consists of four different peptides processed from a single chain precursor. *J Biol Chem* 2005;280:6780–6791.
7. Raben N, Lu N, Nagaraju K, et al. Conditional tissue-specific expression of the acid alpha-glucosidase (GAA) gene in the GAA knockout mice: implications for therapy. *Hum Mol Genet* 2001;10:2039–2047.
8. Raben N, Jatkar T, Lee A, et al. Glycogen stored in skeletal but not in cardiac muscle in acid alpha-glucosidase mutant (Pompe) mice is highly resistant to transgene-encoded human enzyme. *Mol Ther* 2002;6:601–608.
9. Raben N, Danon M, Gilbert AL, et al. Enzyme replacement therapy in the mouse model of Pompe disease. *Mol Genet Metab* 2003;80:159–169.
10. Raben N, Fukuda T, Gilbert AL, et al. Replacing acid alpha-glucosidase in Pompe disease: recombinant and transgenic enzymes are equipotent, but neither completely clears glycogen from type II muscle fibers. *Mol Ther* 2005;11:48–56.
11. Amalfitano A, Bengur AR, Morse RP, et al. Recombinant human acid alpha-glucosidase enzyme therapy for infantile glycogen storage disease type II: results of a phase I/II clinical trial. *Genet Med* 2001;3:132–138.
12. Winkel LP, Kamphoven JH, Van Den Hout HJ, et al. Morphological changes in muscle tissue of patients with infantile Pompe's disease receiving enzyme replacement therapy. *Muscle Nerve* 2003;27:743–751.
13. Winkel LP, Van den Hout JM, Kamphoven JH, et al. Enzyme replacement therapy in late-onset Pompe's disease: a three-year follow-up. *Ann Neurol* 2004;55:495–502.
14. Klinge L, Straub V, Neudorf U, et al. Safety and efficacy of recombinant acid alpha-glucosidase (rhGAA) in patients with classical infantile Pompe disease: results of a phase II clinical trial. *Neuromuscul Disord* 2005;15:24–31.
15. Rando TA, Blau HM. Primary mouse myoblast purification, characterization, and transplantation for cell-mediated gene therapy. *J Cell Biol* 1994;125:1275–1287.
16. Raben N, Nagaraju K, Lee A, et al. Induction of tolerance to a recombinant human enzyme, acid alpha-glucosidase, in enzyme deficient knockout mice. *Transgenic Res* 2003;12:171–178.
17. Maxfield FR. Measurement of vacuolar pH and cytoplasmic calcium in living cells using fluorescence microscopy. *Methods Enzymol* 1989;173:745–771.
18. Diwu Z, Chen CS, Zhang C, et al. A novel acidotropic pH indicator and its potential application in labeling acidic organelles of live cells. *Chem Biol* 1999;6:411–418.
19. Ploug T, van Deurs B, Ai H, et al. Analysis of GLUT4 distribution in whole skeletal muscle fibers: identification of distinct storage compartments that are recruited by insulin and muscle contractions. *J Cell Biol* 1998;142:1429–1446.
20. Kornfeld S. Structure and function of the mannose 6-phosphate/insulinlike growth factor II receptors. *Annu Rev Biochem* 1992;61:307–330.
21. Kabeya Y, Mizushima N, Ueno T, et al. LC3, a mammalian homologue of yeast Apg8p, is localized in autophagosomal membranes after processing. *EMBO J* 2000;19:5720–5728.
22. Weisz OA. Organelle acidification and disease. *Traffic* 2003;4:57–64.
23. Mukherjee S, Ghosh RN, Maxfield FR. Endocytosis. *Physiol Rev* 1997;77:759–803.
24. Dahms NM, Hancock MK. P-type lectins. *Biochim Biophys Acta* 2002;1572:317–340.
25. Kokkonen N, Rivinoja A, Kauppila A, et al. Defective acidification of intracellular organelles results in aberrant secretion of cathepsin D in cancer cells. *J Biol Chem* 2004;279:39982–39988.
26. Bach G, Chen CS, Pagano RE. Elevated lysosomal pH in mucopolidiosis type IV cells. *Clin Chim Acta* 1999;280:173–179.
27. Holopainen JM, Saarikoski J, Kinnunen PK, et al. Elevated lysosomal pH in neuronal ceroid lipofuscinoses (NCLs). *Eur J Biochem* 2001;268:5851–5856.
28. Ghosh P, Dahms NM, Kornfeld S. Mannose 6-phosphate receptors: new twists in the tale. *Nat Rev Mol Cell Biol* 2003;4:202–212.
29. Bonifacino JS. The GGA proteins: adaptors on the move. *Nat Rev Mol Cell Biol* 2004;5:23–32.
30. Puertollano R, Bonifacino JS. Interactions of GGA3 with the ubiquitin sorting machinery. *Nat Cell Biol* 2004;6:244–251.
31. Poussu AM, Thompson PH, Makinen MJ, et al. Vear, a novel Golgi-associated protein, is preferentially expressed in type I cells in skeletal muscle. *Muscle Nerve* 2001;24:127–129.
32. Meyer C, Eskelinen EL, Guruprasad MR, et al. Mu 1A deficiency induces a profound increase in MPR300/IGF-II receptor internalization rate. *J Cell Sci* 2001;114:4469–4476.
33. Mizushima N, Ohsumi Y, Yoshimori T. Autophagosome formation in mammalian cells. *Cell Struct Funct* 2002;27:421–429.
34. Klionsky DJ, Emr SD. Autophagy as a regulated pathway of cellular degradation. *Science* 2000;290:1717–1721.
35. Liou W, Geuze HJ, Geelen MJ, et al. The autophagic and endocytic pathways converge at the nascent autophagic vacuoles. *J Cell Biol* 1997;136:61–70.
36. Berg TO, Fengsrud M, Stromhaug PE, et al. Isolation and characterization of rat liver amphisomes. Evidence for fusion of autophagosomes with both early and late endosomes. *J Biol Chem* 1998;273:21883–21892.
37. Engel AG, Hirschhorn R. Acid maltase deficiency. In: Engel A, Franzini-Armstrong C, eds. *Myology: basic and clinical*. Vol. 2. 2nd ed. New York: McGraw-Hill, 1994:1533–1553.
38. Hesselink RP, Gorselink M, Schaart G, et al. Impaired performance of skeletal muscle in alpha-glucosidase knockout mice. *Muscle Nerve* 2002;25:873–883.
39. Hesselink RP, Van Kranenburg G, Wagenmakers AJ, et al. Age-related decline in muscle strength and power output in acid 1-4 alpha-glucosidase knockout mice. *Muscle Nerve* 2005;31:374–381.
40. Aki T, Yamaguchi K, Fujimiya T, et al. Phosphoinositide 3-kinase accelerates autophagic cell death during glucose deprivation in the rat cardiomyocyte-derived cell line H9c2. *Oncogene* 2003;22:8529–8535.
41. Kondomerkos DJ, Kalamidas SA, Kotoulas OB. An electron microscopic and biochemical study of the effects of glucagon on glycogen autophagy in the liver and heart of newborn rats. *Microsc Res Tech* 2004;63:87–93.
42. Mizushima N, Yamamoto A, Matsui M, et al. In vivo analysis of autophagy in response to nutrient starvation using transgenic mice expressing a fluorescent autophagosome marker. *Mol Biol Cell* 2004;15:1101–1111.
43. Kuncel RW, Bilak MM, Craig SW, et al. Exocytotic “constipation” is a mechanism of tubulin/lysosomal interaction in colchicine myopathy. *Exp Cell Res* 2003;285:196–207.
44. Zhu Y, Li X, McVie-Wylie A, et al. Carbohydrate-remodelled acid alpha-glucosidase with higher affinity for the cation-independent mannose 6-phosphate receptor demonstrates improved delivery to muscles of Pompe mice. *Biochem J* 2005;389:619–628.
45. Ralston E, Lu Z, Ploug T. The organization of the Golgi complex and microtubules in skeletal muscle is fiber type-dependent. *J Neurosci* 1999;19:10694–10705.
46. Ralston E, Ploug T, Kalhovde J, et al. Golgi complex, endoplasmic reticulum exit sites, and microtubules in skeletal muscle fibers are organized by patterned activity. *J Neurosci* 2001;21:875–883.